Investigation of the 2*p* correlation satellites in neon clusters

S. Joshi, S. Barth, S. Marburger, V. Ulrich, and U. Hergenhahn*

Max-Planck-Institut für Plasmaphysik, EURATOM Association, Boltzmannstraße 2,

85748 Garching, Germany

Received 14 December 2005; revised manuscript received 5 May 2006; published 8 June 2006: Physical Review B (Condensed Matter and Materials Physics), **73**, 235404 (2006).

Abstract

Photoelectron spectra of the 2*p* correlation satellites in free Ne clusters have been measured for a number of cluster sizes. With the exception of the least strongly bound prominent satellite line, derived from the $2p^4(^1\mathrm{D})3s$ atomic configuration, the satellites in the cluster show a broadening with the increase of cluster size, but no pronounced energy shift with respect to the atomic lines. The $2p^4(^1\mathrm{D})3s$ satellite has peculiar properties that are analyzed in detail: We find a small monomer-cluster shift of the binding energy, but no splitting of the satellite in a bulk and a surface component. Final state mechanisms that could lead to this behavior, which differs significantly from the main valence photoelectron lines, are discussed.

I. Introduction

Although photoionization primarily results from interaction of a single photon with a single electron, in any complex system additional electrons can rearrange in the ionization process due to electron correlation. This leads to transitions to electronically excited final states, which in a photoelectron spectrum are observed as weak features with a somewhat smaller kinetic energy than the main line from the single electron transition. These weak lines are referred to as ‘satellite’ lines, and their investigation has contributed a lot to the understanding of electron correlation in atomic, molecular and condensed systems. The valence satellite lines of atomic Ne are an example which has been investigated by a

number of different experimental techniques [1-9] and by theory [10], and is well understood today. An important topic of early studies on Ne satellites was the distinction between different satellite production mechanisms [3]. For isolated atoms, satellites are basically produced either by configuration interaction in the ground or final states, or by 'shake-up', which is a relaxation phenomenon.

For bulk matter, additional mechanisms for satellite production are known and have fruitfully been employed to study its electronic structure [11]. In an extended system, one has to distinguish between intrinsic and extrinsic satellites, with the former being produced in the photoionization process and the latter being caused by inelastic losses of the photoelectron on its way through the solid to the surface. Extrinsic losses lead to an inevitable, unstructured background in all photoelectron spectra from solids but can also have a structured fraction. Additional mechanisms for production of intrinsic satellites include charge transfer satellites, which are produced due to screening of the photoion by electrons from neighboring atoms or by delocalized states in the solid.

Since clusters offer a basis to study the evolution of electronic properties from the atom or isolated molecule to the infinite solid, it seems desirable to investigate photoelectron satellites in these systems. However, so far few such studies have been reported. Dobrodey *et al*. have calculated properties of core level photoionization satellites in metal clusters [12-14]. On the experimental side, Hergenhahn *et al.* reported on extrinsic satellites in Ne clusters, which are produced by a fraction of 2*p* photoelectrons that, by inelastic scattering, create an exciton while traveling through the cluster [15].

Another topic in cluster photoionization is surface effects: Since clusters are small, the role of the surface in photoionization can be significant. With respect to bulk and surface cluster sites, photoelectron spectroscopy (PES) provided useful information about energy shifts, intensity variations and relaxation as has been reported [16-20]. Already earlier, the

bulk and surface properties of the rare gas clusters were extensively probed by fluorescence excitation and X-Ray absorption techniques [21-28].

Here, we report on an investigation of the 2*p* correlation satellites in free Ne clusters. Ne clusters were created in a supersonic expansion and were probed by synchrotron radiation of variable photon energy. The focus of our study is to see in detail how the satellite structure reflects the bulk and surface of the clusters. Spectra covering the 2*s* photoelectron main line and a range of 2*p* correlation satellites are presented for a series of cluster sizes. A closer look at the spectra reveals that both the bulk and the surface atoms of the cluster contribute to the satellite intensity. However no surface to bulk energy split of the satellite lines can be observed.

II. Experimental

The experiments were carried out at the undulator beam line U125/1-PGM of the synchrotron radiation source BESSY (Berlin, Germany). The clusters were produced by supersonic expansion of Ne gas through a liquid helium cooled nozzle. A first series of overview spectra was recorded with a nozzle of 100 µm diameter and a half opening angle of 15º (with a length of 275 µm). A series of cluster sizes (65 – 500 atoms) was produced by varying the stagnation pressure at the nozzle from about 400 to 700 mbar and the temperature of the gas from about 62 to 38 K. For further high-resolution measurements, clusters were produced by an 80 µm diameter conical nozzle of half opening angle 15° and a nozzle consisting of a 50 µm cylindrical orifice, which widens to a diameter of 2 mm with an opening angle of 45°, and further extends through the nozzle material to a total length of 3 mm.

The determination of cluster size from the parameters of a supersonic expansion is still a topic of debate, since different methods of size determination did not always arrive at

convergent results. In this article, we will give approximate cluster sizes calculated from the scaling law proposed by Hagena [29], that is, the average cluster size ⟨N⟩ is given by

$$\langle N \rangle = 33 \left(\frac{\Gamma^*}{1000} \right)^{2.35},$$

with the scaling parameter Γ* calculated from

$$\Gamma^* = \frac{p d^{0.85}}{T^{2.2875}} k.$$

Here, *k* collects all material properties and unit conversion constants, and can be calculated as 187.23 [30] when the stagnation pressure *p* is given in mbar, the nozzle diameter *d* in µm and the nozzle temperature T in K. For spectra recorded with a conical nozzle, instead of *d* the equivalent diameter $d_{eq} = 0.736\, d/\tan\alpha$, with α the half opening angle of the cone, has been entered. For the clusters produced by the non conical 50 µm nozzle (see topmost panel of Fig. 4) we give a size estimate based on a comparison to clusters of a similar bulk-to-surface ratio, which were produced by a conical nozzle. This is because Hagena's scaling laws are not applicable to a nozzle of this particular geometry.

Alternatively, one can estimate the size of the clusters from the surface to bulk ratio of the main photoline [18]. We observe that the sizes estimated from the Ne 2*s* signal are larger (by a factor of about 2) compared to the estimates from Hagena's scaling law. The reason of this deviation is not yet completely understood. However, we note that most research on estimation of noble gas cluster sizes was carried out for Ar, not Ne, and Hagena's formulation of the material dependence of the scaling law mostly rested on the comparison to metal clusters [29].

The cluster beam crosses the beam of monochromatized synchrotron radiation after passing a skimmer, which separates the expansion chamber from the main vacuum

chamber. A Scienta ES-200 hemispherical electron analyzer was mounted perpendicular to the light propagation axis and at an angle of 54.7º (magic angle) relative to the horizontal. Linearly polarized synchrotron radiation with a horizontal electric field vector was used. Further details of the apparatus have been published [31, 32].

The cluster beam inevitably contains a fraction of uncondensed Ne atoms (Ne monomers) that were used for binding energy calibration of the cluster features. The binding energy of the atomic 2*s* photoline was set to 48.475 eV [33, 34]. The size dependent series of measurements was corrected for the variation of analyzer transmission with electron kinetic energy, which was determined by measuring atomic Xe 4*d* photolines at a number of energies and normalizing them to some of the $N_{4,5}$ OO Auger lines. Satellite spectra were also recorded for a series of photon energies above the Ne 2*s* ionization threshold up to 120 eV. An overall energy resolution of 80 meV was used for the cluster-size dependent measurements. Detailed spectra of the first prominent satellite were recorded with energy resolutions of 35 and 20 meV, see below. All spectra were subjected to a least squares fit to model the data. A Voigt line shape was used to model the cluster feature while a Gaussian profile was used for the atomic peaks [19]. A linear baseline was fitted simultaneously with the spectra. The residual, that is the difference between the data and the fit, was plotted for each fit in order to judge the quality of the fitting. No significant lifetime broadening of the satellite lines was found.

III. Results

Figure 1 shows Ne photoemission spectra for the monomer and for a series of cluster sizes. The spectra were recorded with a photon energy of 60.5 eV to both cover the kinetic energy regions of the 2*p* correlation satellites and the 2*s* photoline. Obviously, with increasing cluster size the cluster 2*s* line gains intensity while the uncondensed fraction of

the beam, visible as the 2*s* monomer photoline, reduces. The 2*s* cluster photoline is split into contributions of bulk and surface atoms. Our value of the surface-bulk split (0.2 ± 0.03 eV) is consistent with an earlier report by Öhrwall *et al.* [19]. The bulk contribution increases as the cluster size is increased. The atomic satellites are marked in the figure and assigned following the work of Kikas *et al*. [7]. The configuration labels refer to a $1s^2 2s^2 2p^4$ core configuration, which can form a (^{3}P), (^{1}D) or (^{1}S) multiplet state, ordered by increasing binding energy. Ionization of the 2*p* electron can go along with the excitation of another valence electron to a discrete bound 3*s* state, which results in three satellite lines at binding energies of 49.16 eV, 52.14 eV, and 55.88 eV. (The fine-structure splitting due to the 3*s* electron was not resolved.) Within the resolution limit of this work, the $2p^4(^1\text{S})3s$ cannot be distinguished from the $2p^4(^1\text{D})3p(^2\text{P})$ state.

The satellite at a binding energy of 52.14 eV, denoted as (^{1}D)3*s*, shows a distinct cluster component (cluster satellite) shifted by about 200 meV towards lower binding energy. It can be seen that this cluster satellite gains intensity and slightly shifts towards lower binding energy as the cluster size is increased.

The satellites resulting from 2*p* photoionization jointly with valence excitation into a 3*p* state do not show distinct cluster components, which is partly because the cluster satellite components are blended by atomic lines pertaining to other excited configurations. In order to make these cluster satellites more apparent, the monomer signal was subtracted from the spectrum recorded with the largest cluster size, and the difference spectrum is shown in figure 2. It confirms the appearance of cluster satellite lines for electron excitations into the (^{3}P)3*p* and (^{3}P)3*s* states. However, they are too broad for quantitative interpretation. Hence, we will focus on the Ne $2p^4(^1\text{D})3s$ cluster satellite here and carry out a detailed investigation.

Interestingly, no surface-bulk split can be seen in the (^{1}D)3*s* satellite lines in contrast to the photolines. In order to analyze the line profiles in greater detail, we have used a peak fitting routine to model the monomer and cluster components due to the 2*s* main line and the (^{1}D)3*s* satellite. All monomer peaks were modeled by Gaussian profiles, while we decided to model the cluster features by Voigt line shapes, because inner valence holes in clusters can have a finite lifetime due to a fast decay channel made available by the neighboring atoms in the clusters (Interatomic Coulombic Decay), as predicted by theory [35] and proven experimentally in the past few years [36, 37]. The lifetime broadening we observe for the cluster 2*s* main line, and the differences between bulk and surface component, are compatible with published data [19]. However, for the cluster satellite line there was no noticeable gain in the quality of the fit by using a Voigt in comparison to a Gaussian profile apart from a little improvement in description of the low binding energy tail.

The width of the (^{1}D)3*s* satellite line will be discussed next. One can expect quite broad 2*p* photolines because the 2*p* valence states are involved in band formation in neon clusters. Indeed, the 2*p* photoelectron band of Ne clusters, as recorded by our group, looks similar to that of solid neon [38]. Also the inner valence 2*s* photolines are influenced to some extent by broadening due to energy differences between different final states as seen from the larger Gaussian widths of the Voigt profiles. However, the cluster satellite lines which are produced simultaneously with 2*p* photoionization do not show any broadening of a comparable extent. We explain this somewhat surprising result as a final state effect: While the energy difference between surface and bulk states in cluster photoionization results from the different amount of polarization (see below) the broadening within each component has been explained by the formation of ionic molecular oligomers within the cluster as a result of the ionization [39], or, alternatively, by band structure formation in

analogy to the rare gas solids [40]. In the former model, the broadening is the result of the overlap of numerous electronic states of the ionic molecules that are formed, each one also being subject to vibrational broadening. Obviously, no such interaction of the final state with its surroundings takes place for the Ne^+ $2p^4(^1D)3s$ ionic Rydberg state within the clusters. We have calculated the radius of the 3*s* orbital in ionized atomic Ne as 1.65 Å by a single-configuration Hartree-Fock code [41]. In comparison with the interatomic spacing of 3.72 Å [42], the ionic 3*s* orbital radius is small enough to produce little interaction with the neighboring atoms.

Figures 3 (a) and (b) show the results of the peak fits. In order to compare the intensities of the satellite (a) and that of the 2*s* photoline (b), the contributions of the monomer, cluster-bulk, cluster-surface, and cluster-total (bulk + surface) components are plotted for a series of cluster sizes. It can be seen that the surface contribution to the total intensity of the 2*s* photoline outweighs the bulk contribution for cluster sizes smaller than $\langle N \rangle \sim 150$. It is interesting to note that the percentage of satellite peak area (a) develops proportionally to the summed percentage of surface and bulk peak areas of the photoline (b). This suggests that both the surface and the bulk atoms of the cluster contribute to the satellite intensity. In this context it is surprising that this satellite does not show an energy split due to different screening of bulk and surface atoms, similar to the 2*s* photoline, as mentioned above.

In order to further investigate this behavior, we have measured photoelectron spectra of the satellites with better energy resolution. Figure 4 comprises the results of high-resolution $2p^4(^1D)3s$ satellite spectra along with the results of a peak fit for four different expansion conditions, with cluster mean sizes of approximately $\langle N \rangle = 40, 255, 450$ atoms as determined from the scaling law, and 550 atoms as estimated from the comparison to another spectrum (of clusters produced by a conical nozzle) with similar surface to bulk

ratio. The topmost spectrum was recorded with a total apparatus resolution of about 35 meV, while the rest of the spectra were measured with 20 meV resolution. Below the spectrum, the residual, i.e., the difference between the fit and the data is plotted.

In the high resolution spectra measured for larger cluster sizes a second component appears in the cluster satellite peak as a shoulder at the lower binding energy side. From our peak fits we derive an energy difference of about 60 meV with respect to the main peak. The component at lower binding energy (II) shows an increase in the intensity as the cluster size is increased. Straightforwardly, these two components could be interpreted as bulk and surface components of the satellite. However, the intensity ratio of the two components, and the change in intensity with cluster size are neither compatible with an assignment of the weak component as the bulk sites, in analogy to the main line, nor with the reverse assignment. If the components were correctly assigned as bulk and surface, one would have to conclude that the transition amplitude into the satellite state strongly depends on whether this state is excited on the surface of the cluster or in the bulk. While this cannot be ruled out *a priori*, a strong site dependence of the satellite intensity would not be consistent with our earlier observation that the satellite intensity as a function of cluster size behaves like the sum of 2*s* surface and bulk.

Instead, we would like to suggest that these two components arise due to the presence of two types of (local) cluster structures in the beam, i.e., icosahedron (I) and fcc (II). The basis fcc structure is classified as tetrahedron, cuboctahedron etc. depending upon the shape of the cluster. The icosahedral structure does not belong to the fcc basis and according to theoretical studies of the total binding energy, this structure is favored until a certain size (number of atoms) is reached (see e.g. [43]). On the other hand, a structural change towards fcc must take place at some size, since an infinite lattice cannot be built from an icosahedral symmetry, and the fcc structure is also energetically favored for very

large cluster sizes, where surface strain does not play a role. It does not seem likely however, that clusters undergo a global change of structure at some size *N* in order to minimize total energy. Rather a coexistence of several structures has been proposed, as explained below.

To discuss the plausibility of this assignment of features (I) and (II), we briefly refer here some results for Ar clusters, where structural transitions were investigated intensively. According to previous theoretical work [43] and electron diffraction experiments [44] a critical size for a structural change from icosahedron to fcc in Ar clusters is at least 750 atoms. However, recently Kakar *et al.* [45] observed fcc-sensitive maxima in EXAFS measurements on Ar clusters already at $\langle N \rangle \sim 200$. It was suggested that the cluster production method (supersonic expansion) would give rise to defects in the clusters which facilitate growth of fcc crystals for a considerably smaller size. These EXAFS investigations support our hypothesis of fcc structured local environments in the satellite spectra of Ne clusters, which are produced in our work by supersonic expansion similar to the experiment of Kakar *et al*. [45]. It is known that clusters produced by supersonic expansion of gas have a size distribution. Thus, the cluster beam may consist of some bigger clusters (e.g., $\langle N \rangle \sim 750$) which are fcc structured together with small clusters of icosahedral structure. The rise in the intensity of component (II) would then be an indication of an increasing amount of the fcc structured (bigger) clusters against small clusters in the cluster beam as the mean cluster size is increased. The two structural types might even be present simultaneously in one and the same cluster, since the inability of theory to reproduce the latest electron diffraction experiments on Ar clusters was rationalized by the assumption that defects in the icosahedral shaped cluster cores serve to seed further growth of the cluster with a different local structure, most probably fcc [43, 46]. In the EXAFS work mentioned above with respect to clusters smaller than $\langle N \rangle \sim 200$

the authors found that neither icosahedral nor fcc structures are clearly prevalent, and suggested that both may compete in the composition of the clusters. The presence of different local structural motifs in one and the same cluster and within an ensemble of finite temperature clusters of N=201 produced by a Monte Carlo method was recently also found theoretically [47]. Based on this evidence, we tentatively assign component (I) and (II) in the high resolution spectrum of Fig. 4 as due to icosahedral and fcc cluster structures, respectively.

Recent theoretical investigations of nearest neighbor effects on the excited states inside an Ar crystal report that both confinement of the excited orbital and polarization of the surrounding medium influence the excited electron energy [48]. The energy shift increases as the distance between neighboring atoms is reduced. The distance of some of the nearest neighbors is less in case of the icosahedron as compared to the fcc structure, e.g. cuboctahedron. This possibly explains the energy shift of the component II to the smaller binding energy, which arises from the fcc structured clusters in the beam.

Now let us try to understand why no surface to bulk splitting is observable in the cluster satellite spectra. As we have mentioned, the structure of the outer valence photolines in rare gas clusters presumably shows final state effects not explained in detail. In comparison, the inner valence and core vacancy states are simpler to understand [16, 17, 40]. The resulting cationic state is localized, shows few interaction with its surrounding and energy differences between bulk and surface can readily be explained by the smaller amount of polarization screening in the surface sites. If we consider this mechanism only, it would lead to a bulk-surface split for the satellite final states as well. This however might cancel with the different amount of work which is necessary to excite an outer valence electron into the 3*s* Rydberg state within the polarized surrounding of the vacancy. Whether this effect indeed leads to the cancellation of bulk-surface energy differences to

the amount that is seen in our spectra would have to be confirmed by calculation and might be fortuitous, however this effect will in any case diminish the observed splitting.

The observation of a small bulk-surface energy difference of the $2p^4(^1D)3s$ satellite has been qualitatively confirmed by a preliminary ΔSCF calculations of an icosahedral Ne_{13} cluster carried out by N. Kosugi [49]. A mechanism that could lead to this result is the influence of exchange interactions of the lone 3*s* electron with the surroundings. More generally, one can speculate about the specifics of the final state wavefunctions in question. The clusters, although not a long range ordered system, are a first step towards a band structure and this favors a rapid delocalization of the hole (formation of an exciton) due to wave function overlap. Moreover, the wave function overlap is different for different orbitals depending on the local atomic arrangement and the size and symmetry of the atomic wave functions. The valence excited ionic states are again different, both in symmetry and size, and they may form a very different wave function overlap. Furthermore, this may be very different for surface atoms and bulk atoms due to the local surroundings. Therefore, our failure to observe surface-bulk energy split of the first satellite state can be qualitatively understood as the influence of different wave function overlap of surface and bulk excited states. More extended calculations however are needed for a quantitative modeling.

For the ionic Ne 3*s* Rydberg orbital it is still probable that it does not extend beyond the nearest neighbors of the ionized site (Frenkel exciton). The more strongly bound satellites however will involve excitations into delocalized orbitals or Wannier excitons, in condensed matter terminology. For delocalized quantum states, e.g., in quantum dots, which can be treated by a particle-in-a-box model, energy level shifts occur with the size of the system [e.g. 50-53]. This so-called quantum confinement effect can be different for surface states (2-dimensional confinement) as compared to bulk states (3-dimensional

confinement) [22], and thus can lead to a stronger upward shift of binding energies for bulk than surface states. This will not affect the main lines, but may lead to an increase in binding energy for satellites involving excitations to $n > 3$. This will also tend to compensate screening effects.

IV. Summary

In conclusion, we have presented measurements on a series of Ne cluster sizes to investigate 2*p* correlation satellites and the main 2*s* photoline. Apart from cluster-specific excitonic satellites, very less information about atom-specific satellites in rare gas clusters is available and we have tried to shed some light on this aspect here. The cluster satellite lines are comparably less broadened than the main photolines, thus indicating a small interaction of the ionized site with its surroundings in the final state. Interestingly, no surface-bulk energy split is observable for the cluster satellites. Tentative explanations of this fact have been discussed in the text. For the $2p^4(^1\mathrm{D})3s$ cluster satellite, the intensity develops as a sum of cluster bulk and surface intensities. High-resolution data for this line reveal the presence of two components with a small energy difference, which might be attributable to icosahedral and fcc structured regions within the clusters.

Acknowledgements

Useful discussions with E. Umbach and N. Kosugi are gratefully acknowledged. Some helpful comments to the manuscript are due to L. S. Cederbaum. We acknowledge financial support from the Deutsche Forschungsgemeinschaft (DFG).

References:

* Corresponding author, Electronic Address: uwe.hergenhahn@ipp.mpg.de, Mailing Address: Max-Planck-Institut für Plasmaphysik, c/o BESSY mbH, Albert-Einstein-Str. 15, 12489 Berlin, Germany.

[1] P. A. Heimann, C. M. Truesdale, H. G. Kerkhoff, D. W. Lindle, T. A. Ferrett, C. C. Bahr, W. D. Brewer, U. Becker, and D. A. Shirley, Phys. Rev. A **31**, 2260 (1985).

[2] P. A. Heimann, U. Becker, H. G. Kerkhoff, B. Langer, D. Szostak, R. Wehlitz, D. W. Lindle, T. A. Ferrett, and D. A. Shirley, Phys. Rev. A **34**, 3782 (1986).

[3] U. Becker, R. Hölzel, H. G. Kerkhoff, B. Langer, D. Szostak, and R. Wehlitz, Phys. Rev. Lett. **56**, 1120 (1986).

[4] S. Svensson, B. Eriksson, N. Mårtensson, G. Wendin, and U. Gelius, J. Electron Spectrosc. Relat. Phenom. **47**, 327 (1988).

[5] M. O. Krause, S. B. Whitfield, C. D. Caldwell, J.-Z. Wu, P. van der Meulen, C. A. de Lange, and R. W. C. Hansen, J. Electron Spectrosc. Relat. Phenom. **58**, 79 (1992).

[6] G. Kutluk, T. Takaku, M. Kanoo, T. Nagata, E. Shigemasa, A. Yagishita, and F. Koike, J. Phys. B **27**, 5637 (1994).

[7] A. Kikas, S. J. Osborne, A. Ausmees, S. Svensson, O. Sairanen, and S. Aksela, J. Electron Spectrosc. Relat. Phenom. **77**, 241 (1996).

[8] P. Bolognesi, L. Avaldi, D. R. Cooper, M. Coreno, R. Camilloni, and G. C. King, J. Phys. B **35**, 2927 (2002), and references therein.

[9] A. De Fanis, G. Prümper, U. Hergenhahn, M. Oura, M. Kitajima, T. Tanaka, H. Tanaka, S. Fritzsche, N. M. Kabachnik, and K. Ueda, Phys. Rev. A **70**, 040702 (2004); A. De Fanis, G. Prümper, U. Hergenhahn, E. Kukk, T. Tanaka, M. Kitajima, H. Tanaka, S. Fritzsche, N. M. Kabachnik, and K. Ueda, J. Phys. B **38**, 2229 (2005).

[10] R. Colle, A. Mitrushenkov, and S. Simonucci, J. Electron Spectrosc. Relat. Phenom. **123**, 85 (2002), and references therein.

[11] S. Hüfner, *Photoelectron Spectroscopy: Principles and Applications* (Springer-Verlag, Berlin Heidelberg New York, 1995).

[12] N. V. Dobrodey, A. I. Streltsov, L. S. Cederbaum, C. Villani, and F. Tarantelli, J. Chem. Phys. **117**, 3533 (2002).

[13] N. V. Dobrodey, A. I. Streltsov, and L. S. Cederbaum, Phys. Rev. A **65**, 023203 (2002).

[14] N. V. Dobrodey, A. I. Streltsov, and L. S. Cederbaum, Chem. Phys. Lett. **339**, 263 (2001).

[15] U. Hergenhahn, A. Kolmakov, M. Riedler, A. R. B. de Castro, O. Löfken, and T. Möller, Chem. Phys. Lett. **351**, 235 (2002).

[16] O. Björneholm, F. Federmann, F. Fössing, and T. Möller, Phy. Rev. Lett. **74**, 3017 (1995).

[17] O. Björneholm, F. Federmann, F. Fössing, T. Möller, and P Stampfli, J. Chem. Phys. **104**, 1846 (1996).

[18] M. Tchaplyguine, R. R. Marinho, M. Gisselbrecht, J. Schulz, N. Mårtensson, S. L. Sorensen, A. Naves de Brito, R. Feifel, G. Öhrwall, M. Lundwall, S. Svensson, and O. Björneholm, J. Chem. Phys. **120**, 345 (2004).

[19] G. Öhrwall, M. Tchaplyguine, M. Lundwall, R. Feifel, H. Bergersen, T. Rander, A. Lindblad, J. Schulz, S. Peredkov, S. Barth, S. Marburger, U. Hergenhahn, S. Svensson, and O. Björneholm, Phys. Rev. Lett. **93**, 173401 (2004).

[20] M. Tchaplyguine, M. Lundwall, M. Gisselbrecht, G. Öhrwall, R. Feifel, S. Sorensen, S. Svensson, N. Mårtensson, and O. Björneholm, Phys. Rev. A **69**, 03120 (2004).

[21] J. Stapelfeldt, J. Wörmer, and T. Möller, Phys. Rev. Lett. **62**, 98 (1989).

[22] J. Wörmer, M. Joppien, G. Zimmerer, and T. Möller, Phys. Rev. Lett. **67**, 2053 (1991).

[23] M. Joppien, R. Müller, J. Wörmer, and T. Möller, Phys. Rev. B **47**, 12984 (1993).

[24] F. Federmann, O. Björneholm, A. Beutler, and T. Möller, Phys. Rev. Lett. **73**, 1549 (1994).

[25] A. V. Kanaev, M. C. Castex, L. Museur, R. von Pietrowski, and T. Möller, Phys. Rev. Lett. **75**, 2674 (1995).

[26] J. Wörmer, R. Karnbach, M. Joppien, and T. Möller, J. Chem. Phys. **104**, 8269 (1996).

[27] R. v. Pietrowski, M. Rutzen, K. v. Haeften, S. Kakar, and T. Möller, Z. Phys. D **40**, 22 (1997).

[28] T. Laarmann, A. Kanaev, K. von Haeften, H. Wabnitz, R. von Pietrowski, and T. Möller, J. Chem. Phys. **116**, 7558 (2002).

[29] O. F. Hagena, Rev. Sci. Instum. **63**, 2374 (1992) and references therein.

[30] S. Barth, S. Marburger, O. Kugeler, V. Ulrich, S. Joshi, and .U. Hergenhahn, to be published.

[31] S. Marburger, O. Kugeler, and U. Hergenhahn, *Synchrotron Radiation Instrumentation: Eighth International Conference*, edited by T. Warwick, J. Arthur, H. A. Padmore and J. Stöhr, Vol. **705**, p. 1114 (American Institute of Physics, San Francisco, 2003).

[32] S. Barth, S. Joshi, S. Marburger, V. Ulrich, A. Lindblad, G. Öhrwall, O. Björneholm, and U. Hergenhahn, J. Chem. Phys. **122**, 241102 (2005).

[33] W. Persson, Physica Scripta **3**, 133 (1971).

[34] K. Harth, M. Raab, and H. Hotop, Z. Phys. D **7**, 213 (1987).

[35] L. S. Cederbaum, J. Zobeley, and F. Tarantelli, Phys. Rev. Lett. **79**, 4778 (1997); R. Santra, J. Zobeley, and L. S. Cederbaum, Phys. Rev. B **64**, 245104 (2001).

[36] S. Marburger, O. Kugeler, U. Hergenhahn, and T. Möller, Phys. Rev. Lett. **90**, 203401 (2003).

[37] T. Jahnke, A. Czasch, M. S. Schöffler, S. Schössler, A. Knapp, M. Käsz, J. Titze, C. Wimmer, K. Kreidi, R. E. Grisenti, A. Staudte, O. Jagutzki, U. Hergenhahn, H. Schmidt-Böcking, and R. Dörner, Phys. Rev. Lett. **93**, 163401 (2004).

[38] N. Schwentner, F.-J. Himpsel, V. Saile, M. Sikowski, W. Steinmann, and E. E. Koch, Phys. Rev. Lett **34**, 528 (1975).

[39] F. Carnovale, J. B. Peel, R. G. Rothwell, J. Valldorf, and P. J. Kuntz, J. Chem. Phys. **90**, 1452 (1989).

[40] R. Feifel, M. Tchaplyguine, G. Öhrwall, M. Salonen, M. Lundwall, R. R. T. Marinho, M. Gisselbrecht, S. L. Sorensen, A. Naves de Brito, L. Karlsson, N. Mårtensson, S. Svensson, and O. Björneholm, Eur. Phys. J. D **30**, 343 (2004).

[41] R. D. Cowan, *The Theory of Atomic Structure and Spectra* (Berkeley: University of California Press, 1981).

[42] R. Santra, J. Zobeley, L. S. Cederbaum, and N. Moiseyev, Phys. Rev. Lett. **85**, 4490 (2000).

[43] B. W. van de Waal, J. Chem. Phys. **98**, 4909 (1993).

[44] J. Farges, M. F. de Feraudy, B. Raoult, and G. Torchet, J. Chem. Phys. **84**, 3491 (1986).

[45] S. Kakar, O. Björneholm, J. Weigelt, A. R. B. De Castro, L. Tröger, R. Frahm, T. Möller, A. Knop, and E. Rühl, Phys. Rev. Lett. **78**, 1675 (1997).

[46] B. W. van de Waal, J. Chem. Phys. Rev. Lett. **76**, 1083 (1996).

[47] W. Polak and A. Patrykiejew, Phys. Rev. B **67**, 115402 (2003).

[48] J. P. Gauyacq, Phys. Rev. B **71**, 115433 (2005).

[49] N. Kosugi, private communication.

[50] S. Joshi, Ph.D. Thesis, Univ. Würzburg, Germany (2004).

[51] L. E. Brus, J. Chem. Phys. **79**, 5566 (1983).

[52] A. P. Alivisatos, Science, **271**, 933 (1996).

[53] H. Weller, Angew. Chem., Int. Ed. Engl. **32**, 41 (1993).

Figure Captions:

Fig.1

Photoelectron spectra of atomic Ne (bottom) and mixtures of atomic Ne with Ne clusters (other traces). The cluster series was produced by varying the gas pressure and nozzle temperature. The mean cluster size ⟨N⟩ is determined using a scaling law (see text for details). The spectra were recorded with a photon energy of 60.5 eV. Assignments of the Ne 2*p* correlation satellites are taken from Ref. [7]. For a better view of the satellite lines the spectral region from 48.8 eV to 58.2 eV is enlarged.

Fig.2

Spectrum of 2*p* correlation satellites from Ne clusters, inferred by subtracting the scaled atomic contribution from the topmost spectrum in Fig. 1

Fig.3

Relative intensities of monomer and cluster photoelectron lines vs. cluster size for the $2p^4(^1D)3s$ satellite (panel a, top) and the 2*s* main line (panel b, bottom). For the 2*s* main line, the decomposition in bulk and surface component is also given. The percentage of the satellite peak area develops proportionally to the sum of surface and bulk peak areas of the photoline.

Fig. 4

(Color online) Photoemission spectra of Ne $2p^4(^1D)3s$ satellites for four different average cluster sizes, ⟨N⟩=40, ⟨N⟩=255, ⟨N⟩=450, and ⟨N⟩=550. The spectra were recorded with photon energies of 60.5 eV. The fit reveals two cluster satellite components (I-II, solid lines), which are tentatively assigned to a different local ordering in the cluster, as

described in the text. The residuals (i.e., the difference between the data and the fit) are shown below the corresponding spectra.

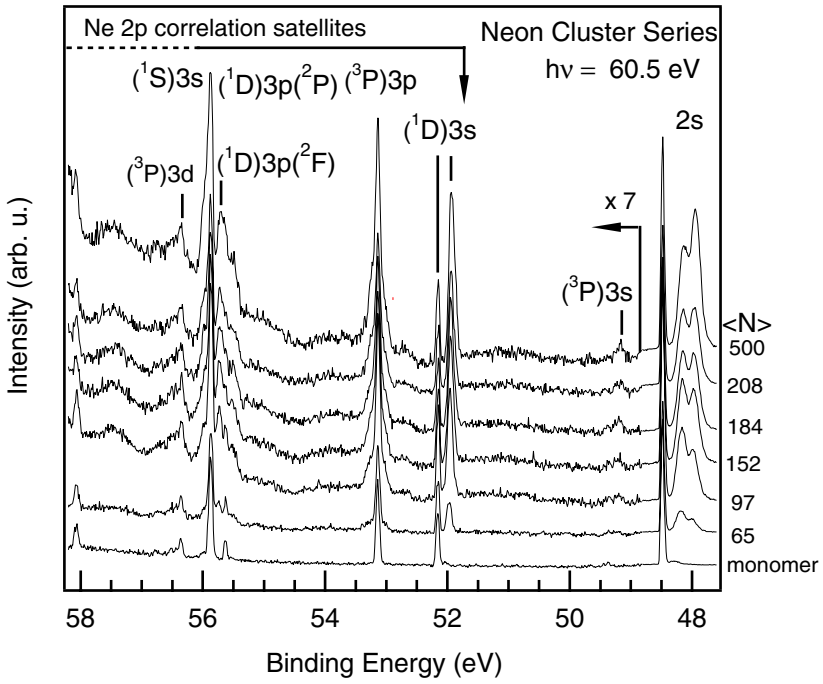

Figure 1

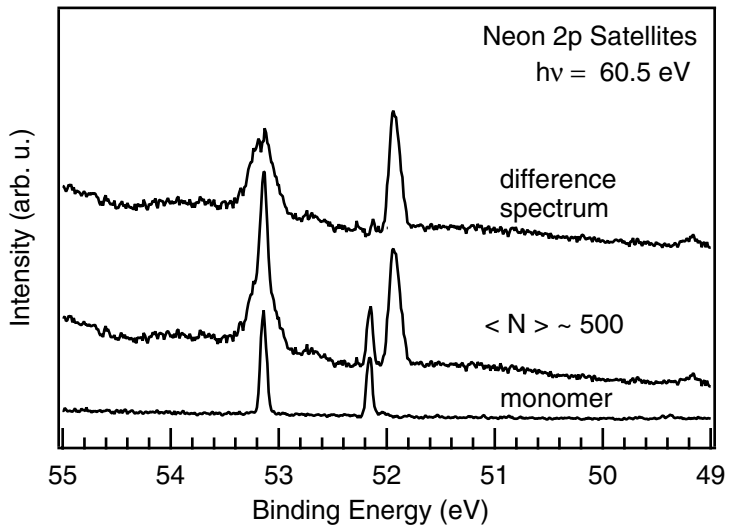

Figure 2

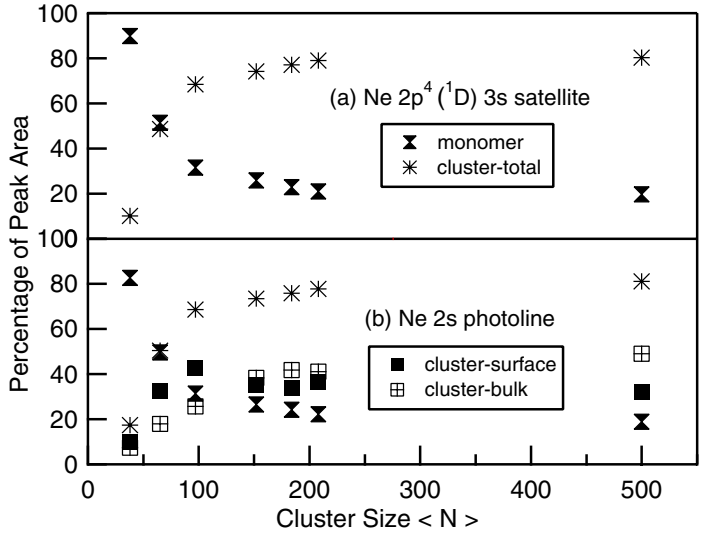

Figure 3

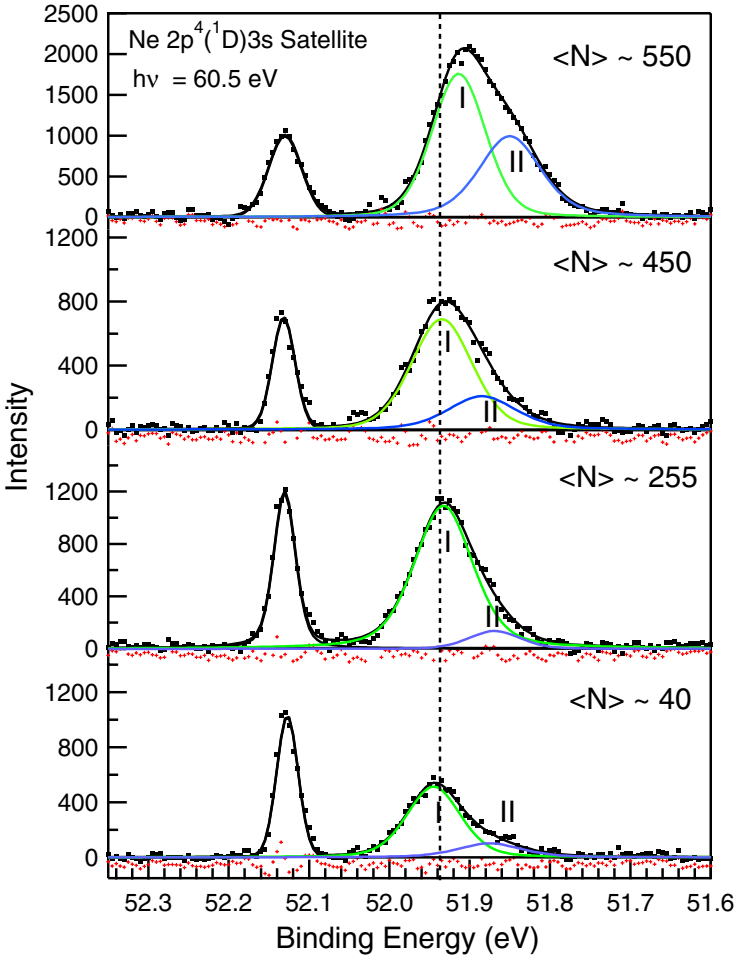

Figure 4